Inorganic Chemistry

Article

pubs.acs.org/IC

New Insight into Self-Irradiation Effects on Local and Long-Range Structure of Uranium−Americium Mixed Oxides (through XAS and XRD)

Florent Lebreton,[†,‡] Philippe M. Martin,[§] Denis Horlait,[†] René Bès,[§] Andreas C. Scheinost,[∥] Andre Rossberg,[∥] Thibaud Delahaye,*[,†] and Philippe Blanchart[‡]

[†]DTEC/SDTC/LEMA, DEN, CEA, F-30207 Bagnols-sur-Cèze Cedex, France

[§]DEC/SECS/LLCC, DEN, CEA, F-13108 Saint-Paul-lez-Durance Cedex, France

[∥]Helmholtz Zentrum Dresden Rossendorf (HZDR), Institute of Radiochemistry, P.O. Box 10119, 01314 Dresden, Germany

[‡]GEMH/ENSCI, 87065 Limoges, France

ABSTRACT: Uranium−americium mixed oxides could be used as transmutation targets to lower Am inventory in spent nuclear fuels. Due to ^{241}Am activity, these materials are subjected to α-self-irradiation which provokes crystallographic disorder. Previous studies on U−Am mixed oxides gave first insight into α-radiation tolerance of these compounds, but have never been carried out for more than a year, whereas these compounds might be stored up to a few years between fabrication and irradiation. In this work, we study effects of self-irradiation on the structure of $U_{1-x}Am_xO_{2\pm\delta}$ solid solutions (x = 0.15 and 0.20) aged 3 to 4 years. Especially, X-ray diffraction and X-ray absorption spectroscopy are combined to observe these effects from both long-range and local perspectives. Results show that the fluorite-type structure of U−Am mixed oxides withstands ^{241}Am α-irradiation without major damage. Despite the increase of interatomic distances and crystallographic disorder observed during the first months of storage, the present results show that a steady state is then reached. Thus, no detrimental factors have been identified in this study in terms of structural damage for several-year storage of $U_{1-x}Am_xO_{2\pm\delta}$ pellets before irradiation. Furthermore, comparison between long-range and local evolution suggests that α-self-irradiation-induced defects are mainly located in low-ordered domains. Based on literature data and present results, the steady state appears related to the equilibrium between radioinduced defect formation and material self-healing.

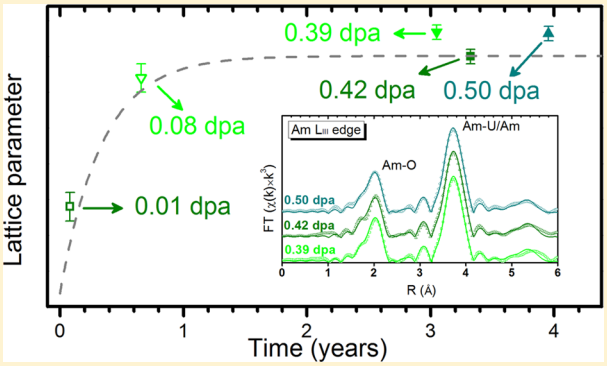

1. INTRODUCTION

The transuranium elements Np, Am, and Cm, usually referred to as minor actinides (MA), are generated in nuclear fuels during in-pile irradiation. Even though they represent a tiny portion of spent fuels (i.e., ∼0.7 wt % of a standard UO_2 fuel irradiated in a pressurized water reactor), their high activity and long half-life make them the highest contributors to radiotoxicity and heat generation of nuclear waste after 100 years (in a scenario integrating plutonium recycling).[1]

Among the considered solutions to manage this particular waste, MA recycling by transmutation into short-lived or stable elements appears to be very promising to reduce MA inventory and consequently the waste volume destined for geological disposal.[2−5] In France, the "heterogeneous" mode is now considered the reference mode for performing MA transmutation.[6,7] It consists of integrating MA in relatively high concentrations (from 7 to 15 atom % of heavy metals) in depleted UO_2-based sintered pellets to perform transmutation in fast neutron reactors (FNR). They are called MA-bearing blankets (MABB), because of their peripheral arrangement in the FNR core. Due to relative abundance and high activity of Am among other MA, heterogeneous mode research is currently focused on recycling of only Am by means of $U_{1-x}Am_xO_{2\pm\delta}$ compounds called AmBB.

Even though irradiation experiments confirmed the feasibility of transmutation through the use of AmBB,[8] consequent work is still needed before an actual industrial deployment.[9,10] In particular, the determination and quantification of elemental mechanisms during solid solution formation and the stability of the latter against α self-irradiation must be explored in detail.

Among studies performed on U−Am mixed oxides, structural properties of these materials were especially investigated, mostly using X-ray diffraction (XRD) and X-ray absorption spectroscopy (XAS). It was notably shown that $U_{1-x}Am_xO_{2\pm\delta}$ solid solutions can be formed at least for $x \leq 0.5$.[11] For samples with $0.1 \leq x \leq 0.2$, XAS studies evidenced a peculiar cationic charge distribution for samples with an oxygen-to-metal (O/M) ratio close to 2 (2.00(1) as obtained by X-ray absorption near edge structure (XANES)). Several authors determined that Am

Received: March 24, 2014
Published: August 27, 2014

   dx.doi.org/10.1021/ic500681k | *Inorg. Chem.* 2014, 53, 9531−9540

Table 1. Sample Characteristics and XRD Refinement Results of the Aged $U_{1-x}Am_xO_{2\pm\delta}$ Samples and of the UO_2 Reference Sample

samples	A	B	C	D	UO_2
Am/(U + Am) ratios (atom %)	15.5(3)	15.5(3)	15.5(3)	20.0(5)	0
aging (days)	1113	1213	1401	1443	
cumulated α doses (10^{18} g^{-1})	1.63(3)	1.77(3)	2.05(4)	2.81(7)	
dpa[a]	0.39(1)	0.42(1)	0.50(1)	0.67(2)	
lattice params (Å)	5.4791(5)	5.4775(5)	5.4792(5)	5.4762(5)	5.4708(5)
interatomic distances (Å)					
An−O1	2.3725(2)	2.3718(2)	2.3726(2)	2.3713(2)	2.3689(2)
An−An1	3.8743(4)	3.8732(4)	3.8744(4)	3.8723(4)	3.8684(4)
An−O2	4.5430(4)	4.5417(4)	4.5431(4)	4.5406(4)	4.5361(4)
crystallite sizes (nm)	>150	>150	>150	133(10)	117(7)
$\langle\varepsilon\rangle$ (10^{-3})	0.6(2)	1.0(2)	0.6(2)	0.3(1)	0.2(1)

[a]Displacement per atom (dpa) values calculated considering 1600 atomic displacements for each ^{241}Am α-decay.[34]

was only present in the trivalent state, while a mixed +IV/+V valence was determined for U.[12−15] The amount of U^{+V} was found to increase with that of Am, as close U^{+V} and Am^{+III} ratios were reported for $U_{1-x}Am_xO_{2\pm\delta}$ samples with $0.1 \leq x \leq 0.2$.[12] This result was quite unexpected, as it strongly differs from those obtained on analogous U−Pu mixed oxides.[16] It was however in agreement with density functional theory calculations performed by Suzuki et al., who predicted the presence of U^{+V} and, mainly, Am^{+III} in a $U_{0.5}Am_{0.5}O_2$ compound.[17] Am thus behaves as many rare-earth elements (Y, Gd, Dy, Sm, Nd, Pr, ...) and more widely elements for which +III is the only oxidation degree available in the solid state and which form mixed-oxide fluorite-type compounds with U. In the mixed oxides obtained, large ionic radii (e.g., Gd^{+III}) are more stable and have higher solubility limits, whereas, for the smaller cations (e.g., Cr^{+III}), hyperstoichiometry of uranium, i.e., presence of U^{+V}, increases the solubility limit.[18]

Concerning the variations of O/M ratios, they are in this case only ensured via changes in the $U^{+IV/+V}$ ratio, as was experimentally observed for U−Am mixed oxides.[19] The fluorite-type structure is thus able to accommodate for the presence of three different oxidation states (+III, +IV, and +V) on the same crystallographic site. Concerning the Np formed by α decay of ^{241}Am, no study of his behavior in the U−Am mixed oxide was performed, but, due to the structural similarities of NpO_2 with UO_2 and $U_{1-x}Am_xO_{2\pm\delta}$, Np can be expected to be present in the fluorite structure in substitution for U/Am.

The structural effects of self-irradiation (mostly induced by the emission of ^{237}Np recoil nuclei from ^{241}Am α-decay)[20] on $U_{1-x}Am_xO_{2\pm\delta}$ solid solutions ($0.075 \leq x \leq 0.500$) were recently studied by Horlait et al.[21] The authors reported that such samples progressively swell, reaching a relative lattice parameter increase $\Delta a/a_0$ of about 0.3% within a few months, according to the equation $\Delta a/a_0 = A(1 - e^{-B\lambda t})$ (with A, the maximum relative swelling, B, a swelling kinetic constant, λ, the ^{241}Am decay constant, and the time t). The Am ratio in the compounds was found to increase the kinetics of lattice parameter expansion, but close kinetics were reported when normalized by the dose rate (which is proportional to the Am ratio as ^{241}Am is the only isotope to have a significant activity in the sample). Neither microstrain increase nor crystallite splitting was evidenced whatever the Am ratio, even though the latter could not be formally ruled out. Microstrain increase with Am ratio was however evidenced and identified as a consequence of the presence of cations with various oxidation states (Am^{+III}, U^{+V}) in amounts increasing with Am ratio. Using XAS, Prieur et al. observed similar swelling between a 20- and a 220-day-old $U_{0.85}Am_{0.15}O_{2\pm\delta}$ sample, as well as, using extended X-ray absorption fine structure (EXAFS), an increase of Debye−Waller factors for each interatomic distance, i.e., an increase of the structural disorder with time.[13] The recovery of self-irradiation-induced lattice expansion with temperature was also studied by Prieur et al. through high-temperature XRD, which allows concluding that recovery of this expansion does not begin under 673 K and is complete at 1373 K.[22]

Self-irradiation studies were, however, limited to one-year-old samples, though AmBB storage between fabrication and irradiation could last several years. Assessing the behavior of AmBB pellets during long storage time requires having data on older samples to confirm their compliance with requirements for irradiations.[6,7] To this end, we report in this work structural investigations by X-ray absorption spectroscopy and powder X-ray diffraction performed on 3- to 4-year-old $U_{1-x}Am_xO_{2\pm\delta}$ sintered samples (with x = 0.15 and 0.20). Obtained results are notably compared to previous studies carried out on similar but more recently prepared samples (less-aged).[12,13,21]

2. EXPERIMENTAL SECTION

2.1. Sample Preparation. Four $U_{1-x}Am_xO_{2\pm\delta}$ sintered samples fabricated in hot cells at the ATALANTE facility were used for this study. Their characteristics are summarized in Table 1. Samples A, B, and C have an Am/(U + Am) ratio of 15.3(5) atom % while that of sample D is 20.0(5) atom %. These compounds, were prepared according to a process already presented in previous publications.[12,23] The latter is notably based on comilling $AmO_{2-\delta}$ and $UO_{2+\delta}$ powders, pelletizing, and reactive sintering at 2023 K during 4 h. Produced pellets were stored at room temperature under air. Samples A and C come from the same starting AmO_2/UO_2 blend, while a different one was employed to fabricate sample B. In consequence, even though the fabrication procedures are the same for the three $U_{0.85}Am_{0.15}O_{2\pm\delta}$ samples, slight differences in impurity content could for example be expected. It is also to be noted that Np is present in the samples as a result of ^{241}Am α decay. When measurements were performed, the Np/(Np + Am) ratio was estimated to be 3.4(3) atom %. A UO_2 sample was used as a reference for EXAFS measurements. It was prepared by sintering following the above-mentioned heat treatment. A lattice parameter of 5.4708(5) Å was obtained, hence an O/M ratio estimated to be 1.998(4) based on results from Teske et al.[24]

XRD characterizations were performed only a few days after the XAS experiment, so sample age of the XRD experiments was considered the same as for XAS. For both XRD and XAS, the sample pellets were crushed and manually ground in an agate mortar. The

dx.doi.org/10.1021/ic500681k | Inorg. Chem. 2014, 53, 9531−9540

XRD sample plate was prepared by mixing a few tens of milligrams of each sample with ~20 mg of Au used as an internal reference (Sigma-Aldrich, purity >99.9%) and an organic grease to adhere the powder to the plate.

For XAS sample preparation, a few milligrams of each powder sample was manually diluted in BN powder by a 10 min manual grinding to ensure homogeneity. The obtained mixture was then pelletized and doubled-sealed in Teflon and polyethylene dedicated containers.

2.2. Data Acquisition and Processing. *2.2.1. XRD.* The XRD device used is a Bruker D8 Advance diffractometer equipped with a Lynx-Eye detector and a Cu source ($K\alpha_1/\alpha_2$ = 1.54056/1.54439 Å), working in $\theta-\theta$ mode. Its main characteristics were recently described.[21] The conditions of diffractogram acquisition were an angular range of 25−120° 2θ and a step size of 0.01° 2θ, thus a total scan duration ≥3 h. Bruker EVA DIFFRACplus and Fullprof Suite software packages were used for data analysis.[25] A Thompson−Cox−Hastings pseudo-Voigt profile function was used for lattice parameter refinement, while microstrain and coherent domain size (i.e., mean crystallite size) were determined by making Williamson−Hall plots.[26,27] The XRD data processing procedure was previously presented in detail.[21]

2.2.2. XAS. XAS experiments were carried out at the European synchrotron radiation facility (ESRF, Grenoble, France) on the Rössendorf Beamline (ROBL) with a storage ring at 6.0 GeV and 170−200 mA. Double-crystal monochromators mounted with Si (111) crystals were used for energy selection. Measurements were performed in both transmission and fluorescence modes, at the U L_{III} (17166 eV), Am L_{III} (18510 eV), U L_{II} (20948 eV), and Np L_{II} (21600 eV) edges. The fluorescence signal was measured with a 13-element Ge solid-state detector using a digital amplifier (XIA). Metallic foils whose K edges are close to the edges of interest, i.e., Y (17038 eV), Zr (17998 eV), and Mo (20000 eV), were used as references for energy calibration. Both XANES and EXAFS spectra were recorded at Am L_{III} and U L_{II} edges, up to k = 18 and 13.5 Å^{-1}, respectively. Spectra at U L_{III} and Np L_{II} were limited to the XANES region as Np amounts in the samples were too high to record EXAFS spectra at U L_{III} but too low to record EXAFS spectra at either Np L_{III} or L_{II} edges. During all the measurements, a He cryostat was used to ensure a sample temperature around 20 K. The thermal agitation contribution to the Debye−Waller factors obtained through EXAFS data refinements is thus greatly reduced and considered negligible, and the latter can be considered only dependent on the structural disorder. Data refinements were performed using the *IFEFFIT*[28,29] software and *FEFF* 8.40 for ab initio calculations of EXAFS spectra.

XANES spectra were normalized using a linear function for pre- and postedge approximation. When necessary, fluorescence spectra were corrected from self-absorption using the *Fluo* algorithm implemented in the ATHENA software.[28,29] Spectra of the following reference compounds (also collected on ROBL at cryogenic temperature) were used for XANES analysis: $U^{+IV}O_2$, $U^{+IV/+V}{}_4O_9$,[30] $U^{+V/+VI}{}_3O_8$,[31] $Np^{+IV}O_2$,[32] $Am^{+IV}O_2$, and a mixed U/Am^{+III} oxalate.[33] White line positions and E_0 (inflection point) were taken as the first zero crossing of the first and second derivatives, respectively. Cation mole fractions were determined using linear combinations of reference spectra to fit experimental normalized absorption spectra of the sample considered.

Fourier transforms of the EXAFS spectra were extracted using a Kaiser−Bessel window between 3.5 and 11.5 Å^{-1} and 3.5 and 14 Å^{-1} for U L_{II} and Am L_{III} edges, respectively (with in both cases a *dk*-factor of 2). A 7.5 Å cluster of the *Fm*-3*m* fluorite-type structure was considered for data fitting, using a (lattice parameter) values obtained by XRD. Each cation is thus theoretically surrounded by 8 O at $a \times \sqrt{3}/4$, 12 U at $a \times \sqrt{2}/2$, 24 O at $a \times \sqrt{11}/4$ and 6 U at a. The four corresponding two-legged paths were included to fit the EXAFS spectra. Two three-legged and two four-legged multiple scattering paths were also chosen, based on their relative high magnitudes. The three-legged paths are Abs−O2−U/Am1−Abs (Abs represents the absorbing atom, and U/Am1 is a cation on the first cation coordination shell of both Abs and O2) and Abs−O2−O1−Abs (O1 is an O anion on the first O coordination shell of both Asb and O2). The four-legged ones are both Abs−O1−Abs−O1−Abs, with angles of 0° (the linear one) or 180° (that for which the first and second O are the same). These multiple-scattering paths were chosen based on their non-negligible relative amplitudes and as they help improving the fit results without the addition of supplementary variables. Fits were performed between 1.6 and 6.0 Å with a k-weight value of 3. The shift in threshold energy ΔE_0 was varied as a global parameter for each spectrum. An amplitude reduction factor $S_0{}^2$ of 0.9 was used, as it is usually done for measurements at An $L_{II/III}$ edges.[12,16]

3. RESULTS AND DISCUSSION

Throughout this section, XRD and XAS data for the samples considered in this study (and whose most relevant characteristics are given in Table 1) are compared to previous results reported by Prieur et al. on less-aged samples[12,13] in order to assess the structural effects of cumulated α dose. Three samples from Prieur et al., hereafter noted A′, B′, and D′, will notably be discussed. Their characteristics are reprinted in Table 2. It is worth noting that all samples were fabricated using the same $UO_{2+\delta}$ and $AmO_{2-\delta}$ powders, samples A, A′, and C being fabricated from a same powder blend, as well as samples B and B′, and samples D and D′, respectively. For analysis of EXAFS results, a UO_2 sample sintered under the same conditions (2023 K under Ar−H_2 (4%) for 4 h) is used as a reference.

Table 2. Main Characteristics of the $U_{1-x}Am_xO_{2\pm\delta}$ Samples Previously Studied by Prieur et al.[12,13]

samples	A′[12,13]	B′[13]	D′[12]
Am/(U + Am) ratios (atom %)	15.5(3)	15.5(3)	20.0(5)
fabrication conditions	similar to A and C	similar to B	similar to D
aging (days)	220	20	550
cumulated α doses (10^{18} g^{-1})	0.32(3)	0.030(3)	1.07(3)
dpa[a]	0.08	0.01	0.25(1)
lattice parameters (Å)	5.476(1)	5.467(2)	5.476(1)

[a]dpa values calculated considering 1600 atomic displacements for each ^{241}Am α-decay.[34] One has to note that the values of 0.03 and 0.28 dpa given for samples B′ and A′,[13] respectively, were here properly recalculated. Likewise, using the original XRD diffractograms, calculated lattice parameters were revised.[35]

3.1. X-ray Diffraction. Powder X-ray diffractograms of the four samples are presented in Figure 1, while Table 1 gathers the refinement results. In all cases, diffraction patterns and diffraction line shapes account for the presence of a sole fluorite-type *Fm*-3*m* $U_{1-x}Am_xO_{2\pm\delta}$ solid solution. This indicates that the fluorite structure is maintained for all samples for the considered accumulated doses of more than 10^{18} α g^{-1} (0.39 to 0.67 dpa) It is consistent with the high resistance of the fluorite structure to self-irradiation.[21,22,34−42]

Structural swelling of the $U_{0.85}Am_{0.15}O_{2\pm\delta}$ compounds is evidenced in Figure 2, which compares lattice parameters of samples A, A′, B, B′, and C to the lattice parameter evolution obtained by Horlait et al.[21] All values are found to be in fair agreement with predicted data. For the older samples (A, B, and C), the lattice parameters no longer evolve after the maximal structural swelling is reached, meaning that the formation kinetics of defect formation from α self-irradiation are the same as the kinetics of defect self-healing.

The refined lattice parameter of the 1443-day-old $U_{0.8}Am_{0.2}O_{2\pm\delta}$ sample is 5.4762(5) Å. It is in agreement with that obtained by Prieur et al. on the same sample 550 days after

dx.doi.org/10.1021/ic500681k | Inorg. Chem. 2014, 53, 9531−9540

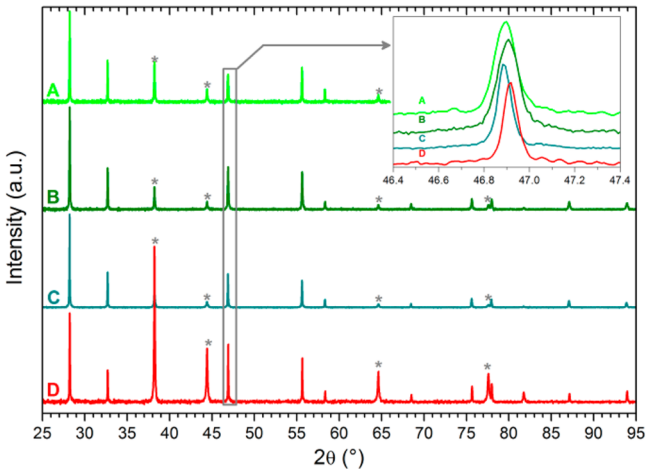

Figure 1. Powder X-ray diffractograms of the samples a few days after XAS experiments showing characteristic lines of the *Fm*-3*m* fluorite structure. Asterisks point out Au pattern. Inset focuses on the (220) line.

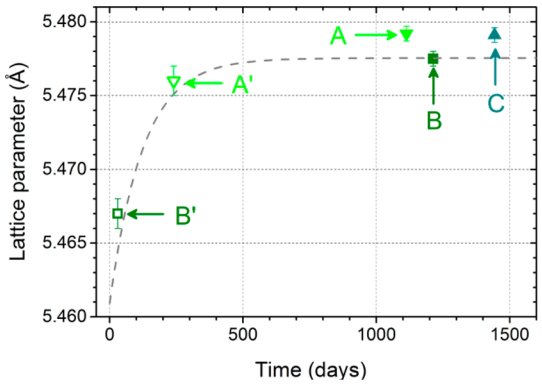

Figure 2. Lattice parameters of the $U_{0.85}Am_{0.15}O_{2\pm\delta}$ samples (filled symbols) compared to those of Prieur et al. (empty symbols).[35] The gray dashed curve is based on data of Horlait et al.[9]

fabrication (5.476(1) Å).[35] These values are ~0.3% higher than that reported by Vespa et al.[43] on a $U_{0.81}Am_{0.19}O_{2\pm\delta}$ sample. This difference is most likely due to self-irradiation effects and would then be consistent with the results of Horlait et al.[21] Another interesting point evidenced by Figure 2 is the lower lattice parameter obtained for sample B than for samples A and C. Likewise, the microstrain $\langle\varepsilon\rangle$ value for sample B ($1.0(2) \times 10^{-3}$) is almost twice those of samples A and C ($0.6(2) \times 10^{-3}$). As a reminder, the three samples were fabricated following the same protocol and from the same UO_2 and AmO_2 starting powders. The discrepancies between sample B and the two others are most probably related to the fact that sample B does not come from the same fabrication batch as samples A and C do. A difference in terms of impurities, brought by grinding and mixing steps, could thus be expected and would be responsible for the above-mentioned difference. $\langle\varepsilon\rangle$, which could be considered an indicator of local variations in lattice parameter, is higher for sample B than for samples A and C. It suggests that the $U_{0.85}Am_{0.15}O_{2\pm\delta}$ crystal structure of sample B is more polluted than those of the two other samples. Unfortunately, due to the limited mass of material available for this study, no impurity content measurements could be performed to confirm this hypothesis.

3.2. XANES. *3.2.1. Am and U Edges.* XANES spectra at the Am L_{III} and U L_{III} edges are presented in Figure 3. Corresponding inflection points and white line positions are summarized in Table 3. XANES spectra at the Am L_{III} edge of the four samples are aligned with that of the Am^{+III} reference. This observation is confirmed by the white line position values, which do not vary by more than 0.2 eV compared to that of the Am^{+III} reference (whereas that of the Am^{+IV} reference is 4.0 eV higher). Linear combination results are also consistent with these observations, as shown in Table 3. Thus, the four samples contain only Am^{+III}. For the U L_{III} edge, all sample spectra are between those of UO_2 (U^{+IV}) and U_4O_9 (1/2 U^{+IV}, 1/2 U^{+V}) reference compounds, as illustrated by the inflection point and white line positions (Table 3). This indicates the presence of U^{+IV} and U^{+V} and excludes the presence of a significant amount of U^{+VI} in the samples. U^{+IV} and U^{+V} mole fractions were consequently determined by linear combination of UO_2 and U_4O_9 reference spectra. Results (Table 4) indicate close amounts of U^{+V} and Am^{+III}, similar to what was already observed on equivalent but less-aged compounds.[12,13] Slightly higher values are obtained for U valence in samples B and C, but it remains impossible to conclude on a strictly higher U^{+V}/U^{+IV} ratio considering the non-negligible uncertainty. Based on the cation mole fractions determined, an O/M (oxygen to metal) ratio of 2.00(1) is calculated for all the samples, with a charge compensation between oxidized U^{+V} and reduced Am^{+III}, similar to what was obtained, notably by DFT calculations, on $U_{1-x}Am_xO_2$ and $U_{1-x}M^{+III}{}_xO_{2\pm\delta}$ compounds.[17,18]

No evolution in Am or U valence was evidenced in the samples over the almost 4-year monitoring of these samples. A recent study showed, through XRD monitoring of powdered $U_{1-x}Am_xO_{2\pm\delta}$ samples under ambient conditions, that the O/M ratio increases during the first days of storage.[21] After this oxidation, O/M ratios close to 2.00 are obtained for Am/(U + Am) ratios comprised between 10 and 20 atom %.[12,44] Present results thus suggest that the O/M ratio of the samples no longer evolves after this initial oxidation, even for a 4-year storage. Notably, α self-irradiation itself does not seem to impact the O/M ratio.

3.2.2. Np Edge. XANES spectra were also recorded at the Np L_{II} edge on samples B and D and are presented with that of a $Np^{+IV}O_2$ reference in Figure 4. Considering the low signal-to-noise ratio due to the limited amount of Np in the samples (between 0.5 and 0.7% of cations), only the white line maximum can be used to determine Np valence state. For both samples this position (21604.6(5) and 21605.0(5) eV for samples B and D, respectively) is close to that of $Np^{+IV}O_2$ (21605.5(5) eV). This indicates that Np is mostly present as Np^{+IV} in samples. It is worth noting that only the Mo K edge could be used for energy calibration of these spectra. Considering the difference between Mo K and Np L_{II} edges (around 1600 eV), the uncertainty on the white line positions is larger for this edge. For both samples, four XANES spectra were merged and plotted in Figure 4. The E_0 deviation between the four spectra was less than 2 eV in both cases. No EXAFS (extended X-ray absorption fine structure) spectra could be obtained at any Np edge, and the elevated noise-to-signal ratio precludes any further interpretation regarding for example the presence of Np in substitution in the U−Am mixed oxide, or aggregated in large Np-rich specific areas as was observed in MA-MOX (MA-bearing mixed U−Pu oxide) fuels.[45]

dx.doi.org/10.1021/ic500681k | Inorg. Chem. 2014, 53, 9531−9540

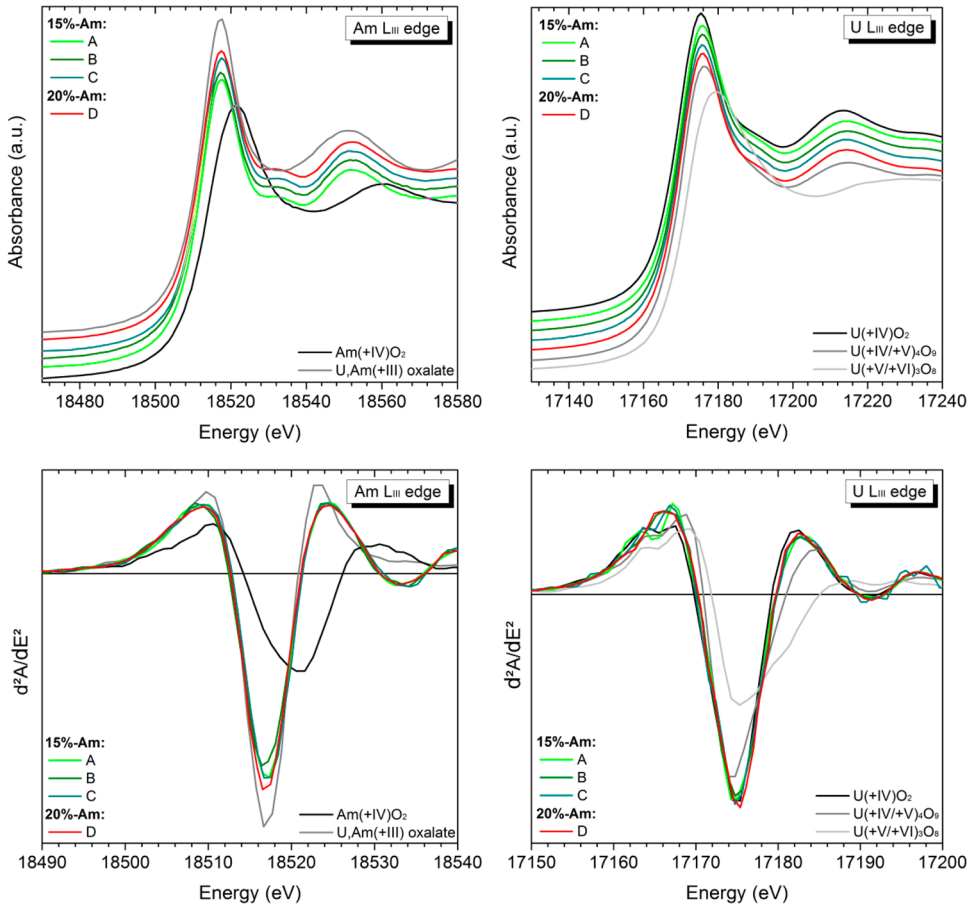

Figure 3. Normalized XANES spectra at Am and U L_{III} edges (to facilitate comparison each subsequent spectrum is shifted by 0.05 on the *y*-axis) and associated second derivatives.

Table 3. Inflection Point (E_0) and White Line (WL) Positions of the XANES Spectra Reported in Figure 3[a]

	Am L_{III} edge		U L_{III} edge	
samples	E_0 (eV)	WL (eV)	E_0 (eV)	WL (eV)
A	18513.0	18517.5	17170.2	17175.9
B	18512.9	18517.4	17170.2	17175.9
C	18513.1	18517.6	17170.0	17175.9
D	18513.0	18517.5	17170.3	17175.9
Am^{+III}[b]	18512.9	18517.7		
$Am^{+IV}O_2$	18514.0	18521.6		
$U^{+IV}O_2$			17169.7	17175.2
$U^{+IV/+V}{}_4O_9$			17170.7	17176.5
$U^{+V/+VI}{}_3O_8$			17171.9	17179.6

[a]All values are given with an uncertainty of 0.2 eV. [b]Am^{+III} reference is $(U^{+IV}{}_{0.9}Am^{+III}{}_{0.1})_2(C_2O_4)_5{\cdot}6H_2O$.[12,33]

Table 4. Mole Fractions and Corresponding O/M Ratios Estimated by Linear Combination of Reference XANES Spectra

	mole fractions (atom %)				
samples	Am^{+III}	Am^{+IV}	U^{+IV}	U^{+V}	O/M ratios
A	15	0	70(2)	15(2)	2.00(1)
B	15	0	68(2)	17(2)	2.00(1)
C	15	0	68(2)	17(2)	2.00(1)
D	20	0	63(2)	17(2)	2.00(1)

3.3. EXAFS. EXAFS spectra at Am L_{III} and U L_{II} edges and their Fourier transforms are presented in Figures 5 and 6, respectively, while Table 5 gathers the fitted structural parameters. In the Fourier transforms, the first peak at ∼1.9−2.0 Å corresponds to the first Am−O or U−O shell, while the second one at ∼3.7 Å mainly corresponds to the nearest Am−U/Am and U−U/Am distances. The good agreement between experimental and fitted data confirms the presence, for each sample, of a single fluorite-type $U_{1-x}Am_xO_{2\pm\delta}$ solid solution. Furthermore, the obtained coordination numbers are consistent (considering the uncertainties) with a fluorite-type structure for each coordination shell considered (i.e., first and second cations and O). The comparisons between the samples and similar but less-aged ones (such as sample B′) or the UO_2 reference sample indicate, however, the occurrence of some structural evolutions during aging.

3.3.1. Interatomic Distances. For the four samples studied, the first shell M−O distance is on average 2.430 Å for Am−O and 2.345 Å for U−O. U−O distances in the samples are thus slightly shorter than that in the UO_2 reference sample (2.355 Å), whereas Am−O are significantly longer. These results are consistent with the cationic charge distribution determined by XANES and the ionic radii of the considered cations in 8-fold coordination.[46]

The presence of U^{+V} thus lowers the U−O distances in the sample in comparison to UO_2, since the U^{+V} ionic radius is smaller (estimated about 0.9 Å) than that of U^{+IV} (1.0 Å). Considering the Am−O distances, their increase is the

dx.doi.org/10.1021/ic500681k | Inorg. Chem. 2014, 53, 9531−9540

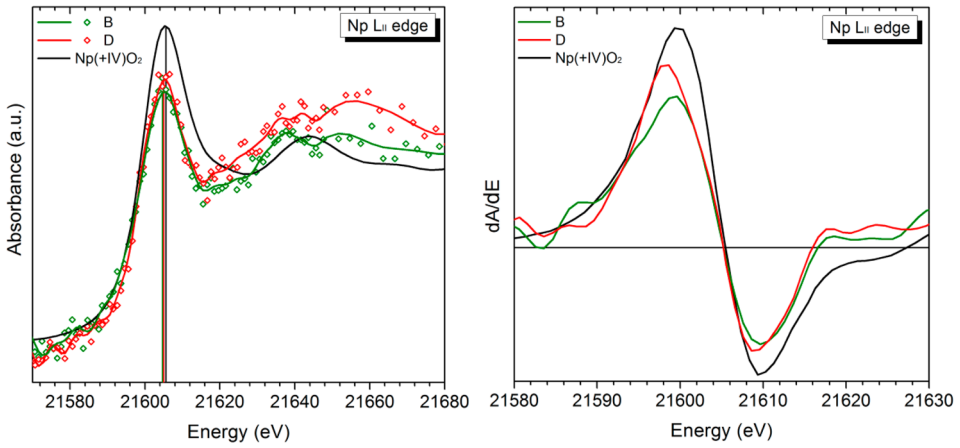

Figure 4. Normalized XANES spectra at Np L_{II} edge of samples B and D compared to that of a NpO_2 reference and associated first derivatives. Symbols represent experimental data, while the colored lines are used to guide the eye. The solid vertical lines around 21605 eV indicate the white line maxima.

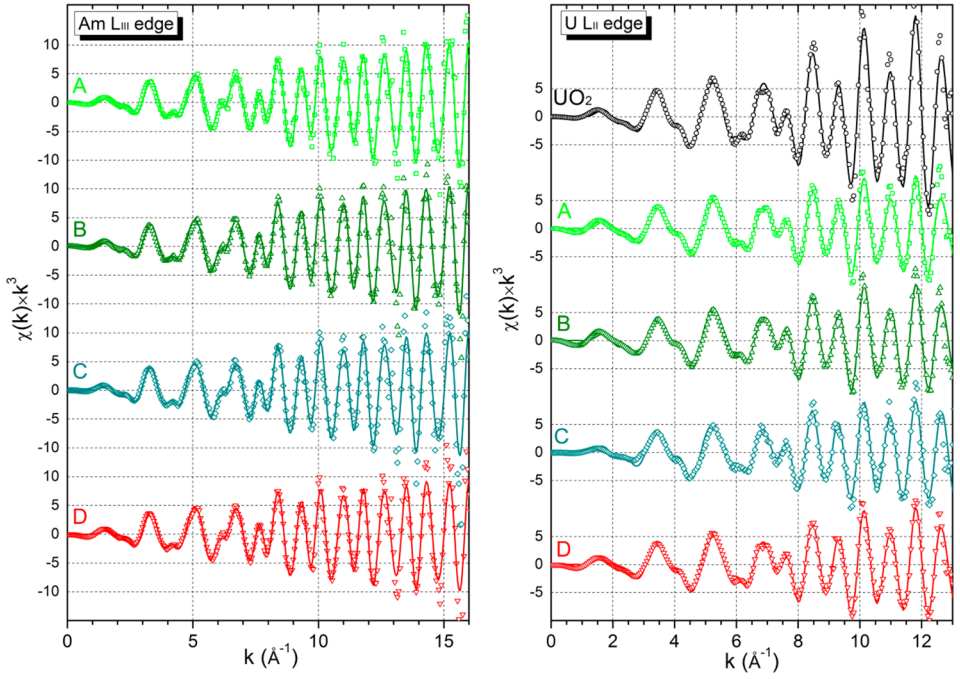

Figure 5. Am L_{III} and U L_{II} edges k^3-weighted EXAFS spectra. Dots correspond to experimental data and solid lines to fitted data.

consequence of the larger ionic radius of Am^{+III} (1.1 Å) compared to those of U^{+IV} and U^{+V}.[46] For the second O coordination shell, the distances obtained are close to that in UO_2 (4.52 Å) for U (about 4.51 Å) but systematically shorter for Am (around 4.49 Å). This difference might not, however, be relevant due to the significant uncertainties for this shell. M−M first distances are all between 3.86 and 3.87 Å, independently of sample age or composition. These distances are in good agreement with those calculated using the lattice parameters determined by XRD measurements (Table 1). Similarly, the second M−M distances, spanning from 5.46 to 5.48 Å, are in fair agreement with the corresponding lattice parameters.

M−O and M−M first and second shell distances of the three $U_{0.85}Am_{0.15}O_{2\pm\delta}$ samples vary less than their respective uncertainties, so they can be considered constant. They are also equal to the M−O and M−M first shell distances determined by Prieur et al.[12] for sample A′ (220 days). All these distances are on average about 0.2% lower for sample B′, aged 20 days. This observation is consistent with XRD results on $U_{0.85}Am_{0.15}O_{2\pm\delta}$, predicting a lattice parameter increase of about 0.20% between 20 days and 220 days and over (but less than 0.05% after 220 days).[21] Thus, during the first year of storage of the $U_{0.85}Am_{0.15}O_{2\pm\delta}$ compounds, self-irradiation induces the progressive lengthening of bonds. A steady state is then reached, when the kinetics of self-healing catch up to those of defect formation by self-irradiation, and the interatomic distances no longer evolve.

3.3.2. Structural Disorder. σ^2 (Debye−Waller factor) values are very close from one sample to another for a given edge and coordination shell. Even though previous studies showed that the higher the Am content, the higher the σ^2 values,[12] no differences associated with Am content are evidenced between the 15 and 20% Am samples. It is presumably due to the small difference in compositions between the samples (5%). These values are, though, higher than those obtained for the UO_2 reference sample. The main differences concern the first O

dx.doi.org/10.1021/ic500681k | Inorg. Chem. 2014, 53, 9531−9540

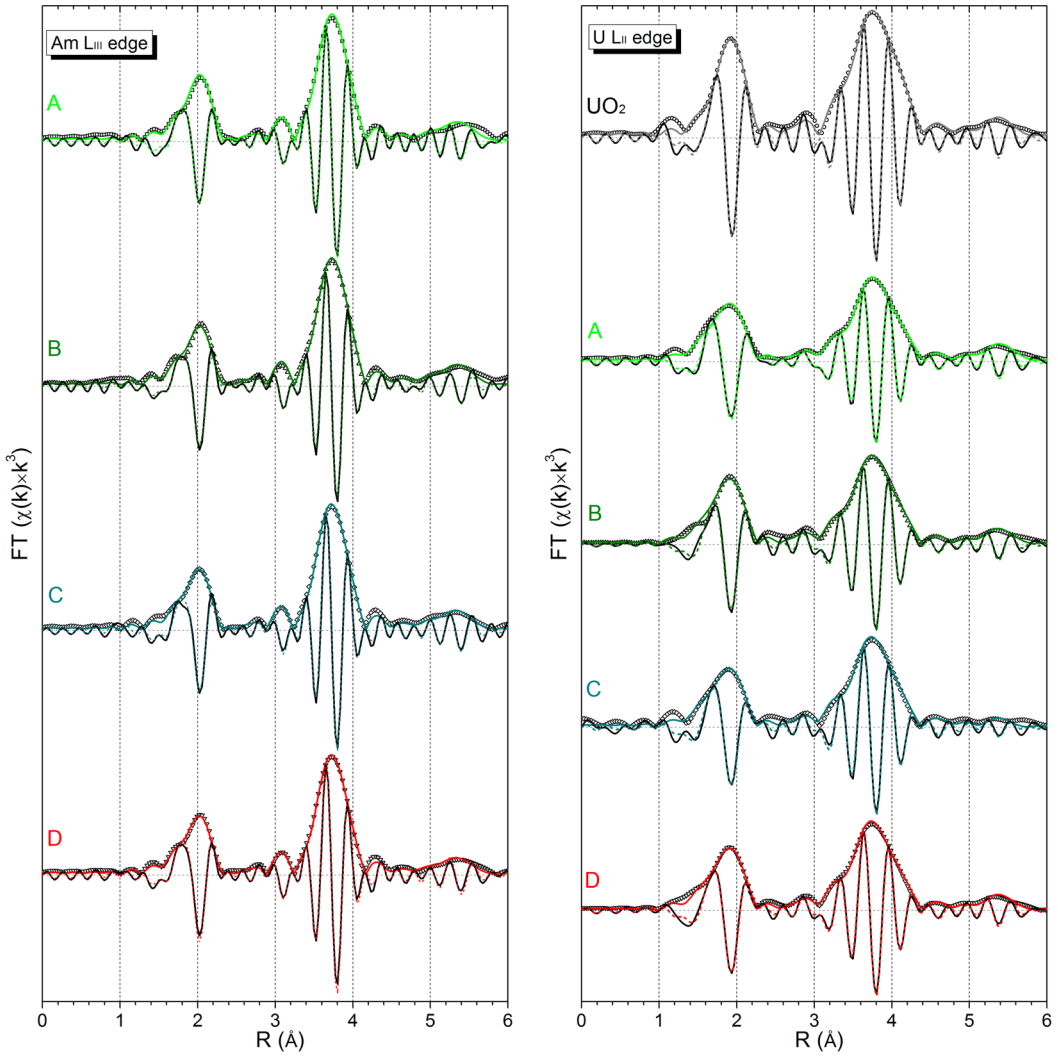

Figure 6. Modulus and imaginary part of Fourier transforms of the k^3-weighted EXFAS spectra at Am L_{III} and U L_{II} edges presented in Figure 5. Black symbols and lines represent the experimental data, whereas gray and colored lines represent the fitting results.

coordination shell. Average values for this shell are significantly higher around U (0.008 Å^2) than around Am (0.005 Å^2), which are both higher than that obtained for the UO_2 reference sample (0.003 Å^2). These differences evidence the increase of the Debye−Waller factor, thus of disorder, resulting from self-irradiation effects (as formerly stated by Prieur et al.[13] and discussed in the next two paragraphs), but are also related to the substitution of Am for U in the structure. Substitutions induce the presence of multivalent cations with different ionic radii, which broadens the cation−O distance distribution, hence the observed increase in disorder of the oxygen sublattice. As the EXAFS results at the U L_{II} edge correspond to two cations, i.e., U^{+IV} and U^{+V}, this disorder appears to be higher around U cations.

For $U_{0.85}Am_{0.15}O_{2\pm\delta}$ samples, σ^2 values of those studied are relatively low, which implies that, despite the cumulated α dose, the $U_{0.85}Am_{0.15}O_{2\pm\delta}$ structure is only slightly disordered. They are also equivalent to those of sample A′ (220 days) and consequently higher (~25%) than those reported for sample B′ (20 days), as formerly stated by Prieur et al.[13] Though ^{241}Am α self-irradiation effects had quantifiable impacts on structural disorder of $U_{0.85}Am_{0.15}O_{2\pm\delta}$ during the first months after synthesis, the present observations indicate that, after reaching the maximal radiation-induced structural swelling, the structural disorder no longer increases. This is consistent with the great resistance of the fluorite structure to α self-irradiation.[21,22,34−42] For sample D, obtained σ^2 values are comparable not only to those reported by Prieur et al. after 550 days[12] but also to those of the aged $U_{0.85}Am_{0.15}O_{2\pm\delta}$ samples.

3.3.3. Influence of the Charge Distribution on the Local Structure. For the four samples studied, XRD and EXAFS results are consistent as they both indicate the conservation of a fluorite-type structure even though U^{+V} and Am^{+III} cations are present. Considering the low sensibility of XRD to light atoms, and thus to the oxygen sublattice, the long-range structure identified by this method almost only corresponds to the cation sublattice, which is thus that of a fluorite-type compound. The differences between U−O1 and Am−O1 (and even probably between U^{+IV}−O1 and U^{+V}−O1) however suggest that some distortions of the oxygen sublattice occurred. Former XAS and neutron studies notably performed on hyperstoichiometric $UO_{2+\delta}$ notably revealed that, during the oxidation of a UO_2 compound, the main structural changes occur in the oxygen sublattice, without influence on the more stable cationic sublattice.[47−52] In the present case, the only modifications from a defect-free fluorite structure are the shortening of the

dx.doi.org/10.1021/ic500681k | Inorg. Chem. 2014, 53, 9531−9540

Table 5. Structural Parameters Obtained by Fitting EXAFS Spectra Reported in Figure 5 at Am L_{III} and U L_{II} Edges of the Aged $U_{1-x}Am_xO_{2\pm\delta}$ and UO_2 Reference Sample

		Am L_{III}				U L_{II}			
samples	shells	R (Å)	N	σ^2 (Å^2)	R-factor	R (Å)	N	σ^2 (Å^2)	R-factor
A, x = 0.15, 1113 d, 0.39 dpa	O1	2.432(5)	7.5(5)	0.0045(5)	0.010	2.348(5)	8.2(5)	0.0085(5)	0.008
	Am/U1	3.865(3)	11.8(5)	0.0031(2)		3.866(3)	12.0(5)	0.0038(2)	
	O2	4.48(2)	22(5)	0.011(2)		4.51(2)	23(5)	0.007(2)	
	Am/U2	5.48(1)	6(1)	0.004(1)		5.47(1)	6(1)	0.003(1)	
B, x = 0.15, 1213 d, 0.42 dpa	O1	2.433(5)	7.6(5)	0.0054(5)	0.012	2.343(5)	7.8(5)	0.0067(5)	0.010
	Am/U1	3.865(3)	11.8(5)	0.0031(2)		3.864(3)	11.9(5)	0.0034(2)	
	O2	4.50(2)	25(5)	0.012(2)		4.51(2)	24(5)	0.008(2)	
	Am/U2	5.47(1)	6(1)	0.003(1)		5.46(1)	6(1)	0.004(1)	
C,[a] x = 0.15, 1401 d, 0.50 dpa	O1	2.426(5)	7.8(5)	0.0054(5)	0.009	2.344(5)	7.9(5)	0.008(1)	0.016
	Am/U1	3.860(3)	11.8(5)	0.0032(2)		3.864(3)	11.8(5)	0.0033(2)	
	O2	4.49(2)	25(5)	0.011(2)		4.52(2)	26(5)	0.010(2)	
	Am/U2	5.47(1)	6(1)	0.003(1)		5.46(2)	5(1)	0.007(2)	
D, x = 0.20, 1443 d, 0.67 dpa	O1	2.430(5)	7.7(5)	0.0055(5)	0.009	2.347(5)	7.9(5)	0.0073(5)	0.006
	Am/U1	3.862(3)	11.8(5)	0.0034(2)		3.865(3)	11.9(5)	0.0034(2)	
	O2	4.49(2)	24(5)	0.012(2)		4.50(2)	24(5)	0.008(2)	
	Am/U2	5.47(1)	6(1)	0.004(1)		5.46(1)	6(1)	0.004(1)	
UO_2	O1					2.355(5)	7.9(5)	0.0031(5)	0.006
	U1					3.866(3)	11.9(5)	0.0015(2)	
	O2					4.52(2)	26(5)	0.005(2)	
	U2					5.46(1)	6(1)	0.003(1)	

[a]Considering EXAFS spectra at the U L_{II} edge of sample C, measurements in fluorescence mode had to be used instead of those in transmission, due to macroscopic defects in the XAS sample. The lower signal-to-noise ratio in such conditions is mainly responsible for the larger uncertainties and R-factor value.

U−O1 distances and a lengthening of the Am−O1 distances, and a slight increase of the associated Debye−Waller compared to a UO_2 compound. In hyperstoichiometric $UO_{2+\delta}$ oxides, the presence of U^{+V} results in the formation of additional U−O distances resulting in an increase of the number of oxygen anions surrounding the U^{+V} cations.[50,51] For the present samples, this was not observed as fairly constant coordination numbers were obtained. Moreover, the first cationic shell, i.e., the first U−An and Am−An distances are similar, meaning that the distortions occur only in the first oxygen shell, which might indicate the presence of U^{+V}−Am^{+III} clusters compensating for the variations in the An−O1 distances. The present experimental data cannot however give any further support to this hypothesis.

These results thus highlight that the two sublattices of the fluorite-type structure can behave quite independently, and that, depending on the method used for the characterization, the information obtained might be relevant only for one, but not for the other. In any case, the peculiar charge distribution observed and its potential effects on the oxygen sublattice certainly influence the way the structure accommodates self-irradiation-induced defects, which is discussed in the next section.

3.3.4. Self-Irradiation Impact on Local and Long-Range Structural Order. The resistance to self-irradiation effects evidenced by these results is in agreement with the great stability of the MO_2-based fluorite-type structure. The latter was often reported as very stable, even up to high equivalent doses.[53] For structures close to the fluorite, it was even suggested that a structural transformation to a defective fluorite induced through irradiation could increase the resistance to amorphization of the considered compounds up to very high doses.[53] More precisely, the stability (i.e., the possibility to accommodate for defect, notably in the oxygen sublattice, rather than undergo amorphization) of fluorite and fluorite-related structures such as those of trivalent-doped MO_2 was found to increase with the closeness of the ionic radii of the considered cations.[53] For U−Am mixed oxides, the similarity between the ionic radii of the three cations present[46] and the consequences of a charge compensation mechanism between U^{+V} and Am^{+III} cations (discussed in the previous section) suggest a high defect accommodation capacity of their structure. This assumption is in accord with the XRD and EXAFS results, in which only low increases of interatomic distances and structural disorders (Debye−Waller factors) were evidenced.

Nevertheless, the increase of Debye−Waller factors during the first months after synthesis appears to be in contradiction with Horlait et al.'s results of XRD monitoring of $U_{1-x}Am_xO_{2\pm\delta}$ compounds ($0.075 \leq x \leq 0.500$) after annealing.[21] Self-irradiation was found to have no quantifiable impact on microstrain ($\langle\varepsilon\rangle$), though Am ratio had a non-negligible impact. $\langle\varepsilon\rangle$ and σ^2 can be considered to be closely related, as they both represent standard deviation or local variation of interatomic distances (as spectra were collected at 15 K, the thermal component in EXAFS data is greatly reduced and can thus be considered negligible). The main difference between them is that $\langle\varepsilon\rangle$ is measured by XRD and thus only for coherent domains (i.e., well-crystallized domains), whereas σ^2-values correspond to the average structural disorder around each cation, thus representative of the entire sample (i.e., coherent and incoherent domains, including defect aggregates and grain boundaries for example). As a consequence, structural disorder induced by self-irradiation in $U_{1-x}Am_xO_{2\pm\delta}$ solid solutions seems to be concentrated in domains having no long-range order. This is also in accord with recent observations made by several research groups[54−57] using computational methods to study formation and subsequent self-healing of self-

dx.doi.org/10.1021/ic500681k | Inorg. Chem. 2014, 53, 9531−9540

irradiation-induced defects in materials with a fluorite-type structure, including notably UO_2. They determined that grain boundaries act as sinks which trap moving atoms and thus point defects induced by collision cascades during α decay. During aging of the samples, structural defects accumulate at grain boundaries (noncoherent diffraction domains). As a consequence, the time necessary to reach the maximum lattice swelling of $U_{1-x}Am_xO_{2\pm\delta}$ compounds may be related to the time necessary for the rate of formation of new defects by self-irradiation to be in equilibrium with the rate of defects reaching noncoherent domains.

No evolutions of Debye−Waller factors are, however, noted after 220 days for $U_{0.85}Am_{0.15}O_{2\pm\delta}$, i.e., at a time when unit cell volume increase through self-irradiation effects is almost stopped. Even though defects still reach noncoherent domains, they do not accumulate there. Some authors indeed determined that defect migration toward grain boundaries can facilitate defect annihilation by interstitial-vacancy recombination near grain boundaries, thus enhancing material self-healing.[54,55] This phenomenon is probably responsible for the observed stabilization of Debye−Waller factors. The defects reaching the noncoherent domains are progressively recovered through interstitial-vacancy recombinations which occur in the vicinity of grain boundaries. Once the kinetics of the latter cancel out those of the former, a steady state is attained, which was observed to occur after at least 220 days in the case of $U_{0.85}Am_{0.15}O_{2\pm\delta}$. Considering that no measurements were performed on such samples aged between 20 and 220 days, it remains impossible to give a more precise approximation of the time necessary to attain this steady state. This compensation process also limits the formation of noncoherent domains, thus protecting the structure against advanced deterioration such as amorphization. The maximum swelling A may be limited by the above-suggested mechanism of enhanced defect healing by grain boundaries. A previous work by Weber[36] is indeed in agreement with that hypothesis, since he reported that, under α irradiation, single crystal UO_2 undergoes 50% more structural swelling than polycrystalline UO_2, probably because of the absence of grain boundaries in single crystals. It is furthermore consistent with the work of Ackland,[55] who discusses the presumed better resistance of nanomaterials to irradiation.

4. CONCLUSIONS

Three- to four-year-old $U_{1-x}Am_xO_{2\pm\delta}$ transmutation targets were analyzed by XRD and XAS to assess the structural effects caused by ^{241}Am α self-irradiation during their aging. By coupling these two techniques, structural self-irradiation effects were studied from both local and long-range points of view. Results show that the fluorite solid solution is retained in spite of the accumulation of α doses up to $\sim 3 \times 10^{18}$ α g^{-1} (i.e., 0.7 dpa). Likewise, the cationic charge distribution appears to be relatively unaffected by α dose accumulation, as it is the same in the 3- to 4-year-old samples as in the less-aged ones (only trivalent Am, U with a mixed +IV/+V valence, leading to O/M values of 2.00(1)). In addition, aged samples exhibit larger interatomic distances than a "fresh" sample.

Concerning structural defects, an increase of Debye−Waller factors is observed using XAS, whereas neither microstrain increase nor crystallite splitting were evidenced by XRD. These results suggest that the self-irradiation-induced structural defects are mostly located in low-ordered domains. These self-irradiation effects are, however, close to those observed in a 220-day-old similar sample, meaning that most of these effects occur during the first months after fabrication concomitantly with a structural swelling. After a few months, the rates of defects reaching noncoherent domains and of subsequent self-healing occurring near grain boundaries compensate for the kinetics of defect formation. An equilibrium state then seems to be established, as no further structural evolution is observed.

In summary, self-irradiation-induced structural evolution in $U_{1-x}Am_xO_{2\pm\delta}$ samples is therefore relatively limited because of the self-healing ability of these compounds. More importantly, none of these evolutions appears to be detrimental to envisaging several-year storage between fabrication and irradiation. However, the accumulated dose remains low compared to those expected for the AmBB under irradiation, and performing the same studies on such samples after irradiation would be of significant interest.

AUTHOR INFORMATION

Corresponding Author

*E-mail: thibaud.delahaye@cea.fr. Tel: +33(0)4-6679-6542.

Notes

The authors declare no competing financial interest.

ACKNOWLEDGMENTS

The authors are thankful to N. Astier, M. Bataille, P. Coste, and D. Prieur for sample preparation and handling, to L. Guérin for performing gamma spectrometry, and to P. Colomp and C. Guihard for organizing sample transportation. Thanks also have to be addressed to N. T. Reilly for her advice. F.L. and D.H. acknowledge the CEA PACFA program for financial support through Ph.D. and postdoctoral fellowship funding, respectively. The authors also thank the ESRF for provision of synchrotron radiation facilities.

REFERENCES

(1) Salvatores, M. *Prog. Nucl. Energy* **2002**, *40*, 375−402.
(2) Warin, D. *J. Nucl. Sci. Technol.* **2007**, *44*, 410−414.
(3) Grouiller, J.-P.; Pillon, S.; de Saint Jean, C.; Varaine, F.; Leyval, L.; Vambenepe, G.; Carlier, B. *J. Nucl. Mater.* **2003**, *320*, 163−169.
(4) Ronchi, C.; Ottaviani, J. P.; Degueldre, C.; Calabrese, R. *J. Nucl. Mater.* **2003**, *320*, 54−65.
(5) Lebreton, F.; Prieur, D.; Horlait, D.; Delahaye, T.; Jankowiak, A.; Léorier, C.; Jorion, F.; Gavilan, E.; Desmoulière, F. *J. Nucl. Mater.* **2013**, *438*, 99−107.
(6) Prieur, D.; Jankowiah, A.; Delahaye, T.; Herlet, N.; Dehaudt, P.; Blanchart, P. *J. Nucl. Mater.* **2011**, *414*, 503−507.
(7) Delahaye, T.; Lebreton, F.; Horlait, D.; Herlet, N.; Dehaudt, P. *J. Nucl. Mater.* **2013**, *432*, 305−312.
(8) D'Agata, E.; Hania, P. R.; Bejaoui, S.; Sciolla, C.; Wyatt, T.; Hannink, M. H. C.; Herlet, N.; Jankowiak, A.; Klaassen, F. C.; Lapetite, J.-M.; Boomstra, D. A.; Phelip, M.; Delage, F. *Ann. Nucl. Energy* **2013**, *62*, 40−49.
(9) Salvatores, M.; Palmiotti, G. *Prog. Part. Nucl. Phys.* **2011**, *66*, 144−166.
(10) Tuček, K.; Tsige-Tamirat, H.; Ammirabile, L.; Lázaro, A.; Grah, A.; Carlsson, J.; Döderlein, C.; Oettingen, M.; Fütterer, M. A.; D'Agata, E.; Laurie, M.; Turba, K.; Ohms, C.; Nilsson, K.-F.; Hähner, P. *Nucl. Eng. Des.* **2013**, *265*, 1181−1193.
(11) Lebreton, F.; Horlait, D.; Delahaye, T.; Blanchart, P. *J. Nucl. Mater.* **2013**, *439*, 99−102.
(12) Prieur, D.; Martin, P. M.; Jankowiak, A.; Gavilan, E.; Scheinost, A. C.; Herlet, N.; Dehaudt, P.; Blanchart, P. *Inorg. Chem.* **2011**, *50*, 12437−12445.
(13) Prieur, D.; Martin, P.; Lebreton, F.; Delahaye, T.; Banerjee, D.; Scheinost, A. C.; Jankowiak, A. *J. Nucl. Mater.* **2013**, *434*, 7−16.

(14) Nishi, T.; Nakada, M.; Suzuki, C.; Shibata, H.; Okamoto, Y.; Akabori, M.; Hirata, M. *J. Nucl. Mater.* **2011**, *418*, 311−312.
(15) Prieur, D.; Lebreton, F.; Martin, P. M.; Jankowiak, A.; Delahaye, T.; Dehaudt, P.; Blanchart, P. *J. Eur. Ceram. Soc.* **2012**, *32*, 1585−1591.
(16) Martin, P.; Grandjean, S.; Valot, C.; Carlot, G.; Ripert, M.; Blanc, P.; Hennig, C. *J. Alloys Compd.* **2007**, *444*−*445*, 410−414.
(17) Suzuki, C.; Nishi, T.; Nakada, M.; Tsuru, T.; Akabori, M.; Hirata, M.; Kaji, Y. *J. Phys. Chem. Solids* **2013**, *74*, 1769−1774.
(18) Middleburgh, S. C.; Parfitt, D. C.; Grimes, R. W.; Dorado, B.; Bertolus, M.; Blair, P. R.; Hallstadius, L.; Backman, K. *J. Nucl. Mater.* **2012**, *420*, 258−261.
(19) Prieur, D.; Martin, P.; Lebreton, F.; Delahaye, T.; Banerjee, D.; Scheinost, A. C.; Jankowiak, A. *J. Nucl. Mater.* **2013**, *434*, 7−16.
(20) Wiss, T. In *Comprehensive Nuclear Materials*; Konings, R. J. M., Ed.; Elsevier: Oxford, 2012; pp 465−480.
(21) Horlait, D.; Lebreton, F.; Roussel, P.; Delahaye, T. *Inorg. Chem.* **2013**, *52*, 14196−14204.
(22) Prieur, D.; Pagliosa, G.; Spino, J.; Caciuffo, R.; Somers, J.; Eloirdi, R. *J. Solid State Chem.* **2013**, *199*, 334−337.
(23) Prieur, D.; Jankowiak, A.; Leorier, C.; Herlet, N.; Donnet, L.; Dehaudt, P.; Maillard, C.; Laval, J.-P.; Blanchart, P. *Powder Technol.* **2011**, *208*, 553−557.
(24) Teske, K.; Ullmann, H.; Rettig, D. *J. Nucl. Mater.* **1983**, *116*, 260−266.
(25) Rodríguez-Carvajal, J. *Phys. B* **1993**, *192*, 55−69.
(26) Williamson, G. K.; Hall, W. H. *Acta Metall.* **1953**, *1*, 22−31.
(27) Shao, Z.; Saitzek, S.; Ferri, A.; Rguiti, M.; Dupont, L.; Roussel, P.; Desfeux, R. *J. Mater. Chem.* **2012**, *22*, 9806−9812.
(28) Newville, M. *J. Synchrotron Radiat.* **2001**, *8*, 322−324.
(29) Ravel, B.; Newville, M. *J. Synchrotron Radiat.* **2005**, *12*, 537−541.
(30) Desgranges, L.; Baldinozzi, G.; Rousseau, G.; Niepce, J.; Calvarin, G. *Inorg. Chem.* **2009**, *48*, 7585−7592.
(31) Kvashnina, K. O.; Butorin, S. M.; Martin, P.; Glatzel, P. *Phys. Rev. Lett.* **2013**, *111*, 253002.
(32) Chollet, M.; Belin, R. C.; Richaud, J.-C.; Martin, P. M.; Reynaud, M.; Scheinost, A. C.; Hennig, C. In *American Nuclear Society 2013 Annual Meeting*; Atlanta, GA, USA, June 16−20, 2013.
(33) Grandjean, S.; Arab-Chapelet, B.; Robisson, A. C.; Abraham, F.; Martin, P.; Dancausse, J.-P.; Herlet, N.; Léorier, C. *J. Nucl. Mater.* **2009**, *385*, 204−207.
(34) Wiss, T. In *Comprehensive Nuclear Materials*; Konings, R. J. M., Ed.; Elsevier: Oxford, 2012; pp 465−480.
(35) Prieur, D. *Elaboration de combustible à base d'oxydes d'uranium et d'américium: modélisation thermodynamique et propriétés des matériaux*. Ph.D Thesis, Université de Limoges, 2011.
(36) Weber, W. J. *Radiat. Eff.* **1983**, *77*, 295−308.
(37) Matzke, H.; Kinoshita, M. *J. Nucl. Mater.* **1997**, *247*, 108−115.
(38) Ewing, R. C.; Weber, W. J. In *The Chemistry of the Actinide and Transactinide Elements*; Springer: New-York, 2011; pp 3813−3887.
(39) Lebreton, F.; Belin, R. C.; Delahaye, T.; Blanchart, P. *J. Solid State Chem.* **2012**, *196*, 217−224.
(40) Chikalla, T. D.; Eyring, L. *J. Inorg. Nucl. Chem.* **1968**, *30*, 133−145.
(41) Hurtgen, C.; Fuger, J. *Inorg. Nucl. Chem. Lett.* **1977**, *13*, 179−188.
(42) Garrido, F.; Vincent, L.; Nowicki, L.; Sattonnay, G.; Thomé, L. *Nucl. Instrum. Methods Phys. Res., Sect. B* **2008**, *266*, 2842−2847.
(43) Vespa, M.; Rini, M.; Spino, J.; Vitova, T.; Somers, J. *J. Nucl. Mater.* **2012**, *421*, 80−88.
(44) Prieur, D.; Martin, P. M.; Lebreton, F.; Delahaye, T.; Jankowiak, A.; Laval, J.-P.; Scheinost, A. C.; Dehaudt, P.; Blanchart, P. *J. Solid State Chem.* **2012**, *194*, 206−211.
(45) Lebreton, F.; Prieur, D.; Jankowiak, A.; Tribet, M.; Leorier, C.; Delahaye, T.; Donnet, L.; Dehaudt, P. *J. Nucl. Mater.* **2012**, *420*, 213−217.
(46) Shannon, R. D. *Acta Crystallogr., Sect. A* **1976**, *32*, 751−767.
(47) Willis, B. T. M. *Nature* **1963**, *197*, 755−756.
(48) Bevan, D. J. M.; Grey, I. E.; Willis, B. T. M. *J. Solid State Chem.* **1986**, *61*, 1−7.
(49) Garrido, F.; Ibberson, R. M.; Nowicki, L.; Willis, B. T. M. *J. Nucl. Mater.* **2003**, *322*, 87−89.
(50) Conradson, S. D.; Manara, D.; Wastin, F.; Clark, D. L.; Lander, G. H.; Morales, L. A.; Rebizant, J.; Rondinella, V. V. *Inorg. Chem.* **2004**, *43*, 6922−6935.
(51) Conradson, S. D.; Begg, B. D.; Clark, D. L.; den Auwer, C.; Ding, M.; Dorhout, P. K.; Espinosa-Faller, F. J.; Gordon, P. L.; Haire, R. G.; Hess, N. J.; Hess, R. F.; Webster Keogh, D.; Lander, G. H.; Manara, D.; Morales, L. A.; Neu, M. P.; Paviet-Hartmann, P.; Rebizant, J.; Rondinella, V. V.; Runde, W.; Drew Tait, C.; Kirk Veirs, D.; Villella, P. M.; Wastin, F. *J. Solid State Chem.* **2005**, *178*, 521−535.
(52) Conradson, S. D.; Durakiewicz, T.; Espinosa-Faller, F. J.; An, Y. Q.; Andersson, D. A.; Bishop, A. R.; Boland, K. S.; Bradley, J. A.; Byler, D. D.; Clark, D. L.; Conradson, D. R.; Conradson, L. L.; Costello, A. L.; Hess, N. J.; Lander, G. H.; Llobet, A.; Martucci, M. B.; Mustre de Leon, J.; Nordlund, D.; Lezama-Pacheco, J. S.; Proffen, T. E.; Rodriguez, G.; Schwarz, D. E.; Seidler, G. T.; Taylor, A. J.; Trugman, S. A.; Tyson, T. A.; Valdez, J. A. *Phys. Rev. B* **2013**, *88*, 115135.
(53) Sickafus, K. E.; Valdez, J. A.; Williams, J. R.; Grimes, R. W.; Hawkins, H. T. *Nucl. Instrum. Methods Phys. Res., Sect. B* **2002**, *191*, 549−558.
(54) Bai, X.-M.; Voter, A. F.; Hoagland, R. G.; Nastasi, M.; Uberuaga, B. P. *Science* **2010**, *327*, 1631−1634.
(55) Ackland, G. *Science* **2010**, *327*, 1587−1588.
(56) Van Brutzel, L.; Vincent-Aublant, E.; Delaye, J.-M. *Nucl. Instrum. Methods Phys. Res., Sect. B* **2009**, *267*, 3013−3016.
(57) Uberuaga, B. P.; Andersson, D. A.; Stanek, C. R. *Curr. Opin. Solid State Mater. Sci.* **2013**, *17*, 249−256.